Resonance Raman Spectroscopy of Cytochrome *c* Peroxidase Single Crystals on a Variable-Temperature Microscope Stage†

Giulietta Smulevich,*,‡ Yang Wang,§ Steven L. Edwards,∥ Thomas L. Poulos,∥ Ann M. English,⊥ and Thomas G. Spiro*,§

Dipartimento di Chimica, Università di Firenze, Via G. Capponi 9, 50121 Firenze, Italy, Department of Chemistry, Princeton University, Princeton, New Jersey 08544-1009, Center for Advanced Research in Biotechnology of the Maryland Biotechnology Institute, University of Maryland, Shady Grove, 9600 Gudelsky Drive, Rockville, Maryland 20850, and Department of Chemistry, Concordia University, Montreal, Quebec, Canada H3G 1M8

Received February 15, 1989; Revised Manuscript Received November 1, 1989

ABSTRACT: Good quality resonance Raman (RR) spectra have been obtained for cytochrome *c* peroxidase single crystals (0.2 × 0.5 × 1 mm) lying on their 110 faces on a microscope stage. Crystal orientation and polarization effects are observed which differentiate the RR bands on the basis of the symmetries of the porphyrin vibrational modes. The measured depolarization ratios are accurately calibrated for isolated bands of both totally symmetric and non totally symmetric modes by using a model of D_{4h} chromophores in an oriented gas using the crystal structure atomic coordinates. The calculations indicate that the electronic transition moments are approximately along the lines connecting the methine bridges, suggesting an electronic steering effect of the vinyl groups. Deviations are observed for bands associated with the porphyrin ν_{10} and the vinyl C=C stretching modes, which may be due to their near-resonant interaction. The band frequencies correspond to those of a five-coordinate high-spin Fe^{III} heme, as previously observed in solution, consistent with the X-ray structure showing the Fe atom to be out of the heme plane on the proximal side with a distal water molecule located at a nonbonded distance, 2.4 Å. The temperature dependence of the RR spectrum was determined with a Joule-Thompson cryostat on crystals sealed in glass capillaries. As the temperature is lowered, the spectrum converts to one characteristic of a low-spin Fe^{III} heme. The conversion, which is readily reversible, is quite gradual. It is detectable at −50 °C but is incomplete even at −190 °C. A temperature effect on the protein structure is proposed which permits the Fe atom to approach the heme plane and bind the distal water molecule, or the distal histidine.

Since information on the molecular architecture of proteins depends overwhelmingly on X-ray crystal structure determinations, it is highly desirable to develop spectroscopic techniques capable of comparing proteins in single crystals and in solution or in their biological matrices. Raman spectroscopy is an attractive candidate for such comparisons because the vibrational spectrum is sensitive only to the local environment of the molecular oscillators and is independent of the medium. The vibrational frequencies are sensitive to molecular structure, and one can probe for specific chromophoric sites via the resonance Raman effect by tuning the wavelength of the exciting light to an appropriate electronic transition (Carey, 1982). In the crystal the chromophores are in general vibrationally well isolated from one another. The properties of the molecular scattering tensor can be therefore calculated from the properties of the crystal scattering tensor by means of the geometric relationships between the molecular and the crystal axes. Laser light sources make it possible to obtain a Raman spectrum in backscattering from a crystal face which is as small as the laser beam cross section. Nevertheless, protein crystals are a formidable challenge to Raman spectroscopists because they are fragile and easily destroyed by the laser beam, especially in the case of resonance Raman spectroscopy when the sample absorbs the light and is heated by it. Despite these problems, Champion and co-workers (Morikis et al., 1988) have recently shown that good quality resonance Raman spectra can be obtained on single crystals of myoglobin and have given a detailed treatment of orientation and polarization effects (Sage et al., 1989).

It occurred to us that technical problems could be minimized by using a microscope. Raman microprobes are now in widespread use for the examination of selected microscopic areas of samples but have not to our knowledge been applied to protein crystals. Since these are often irregularly shaped objects, it is advantageous to be able to select a microscopic area of good optical quality. The high light-gathering power of the microscope objective permits the use of low laser powers, thereby limiting the extent of laser-induced damage. Crystal orientation information is reduced to two dimensions on a microscope stage versus three dimensions for a crystal mounted on a goniometer, but since many crystals are obtained as thin plates, the missing orientation might be inaccessible in any event. The stage can be cooled, further limiting laser damage and allowing for studies of the temperature dependence of protein structure. Application of a liquid nitrogen cooled microscope for resonance Raman spectroscopic studies of visual cone cells has recently been reported (Loppnow & Mathies, 1989; Loppnow et al., 1989).

In this paper we describe a Raman microscope suitable for single-crystal studies and apply it to single crystals of cytochrome *c* peroxidase (CCP) (Yonetani, 1976). Good quality spectra were obtained, and substantial orientation and polarization effects are seen which discriminate among the RR bands of the heme group on the basis of the symmetries of the porphyrin vibrations. The vibrational frequencies are characteristic of five-coordinate high-spin Fe^{III} heme. This result

† This work was supported by NIH Grant GM33576 (to T.G.S.), NATO Grant 86/0453 (to G.S., A.M.E., and T.G.S.), and NSF Grant DMB-8716316 (to T.L.P.).

* Authors to whom correspondence should be addressed.
‡ Università di Firenze.
§ Princeton University.
∥ Center for Advanced Research in Biotechnology.
⊥ Concordia University.

0006-2960/90/0429-2586$02.50/0

is of interest because the X-ray structure (Poulos et al., 1980; Finzel et al., 1984) shows a water molecule distal to the heme group but at a distance, 2.4 Å, which is too long for chemical bonding, and the Fe atom lies out of the plane on the proximal side. A six-coordinate high-spin heme can be seen in CCP mutants (Smulevich et al., 1988) and in solutions of native CCP at low pH (Hashimoto et al., 1982a,b; Smulevich et al., 1986a,b), but in the latter case the six-coordinate adduct seems to be the result of an aging process (Yonetani & Anni, 1987; Dasgupta et al., 1989). The present result confirms that the five-coordinate structure is characteristic of native CCP, in crystals or solution, near neutral pH.

In view of the finding by Yonetani and Anni (1987) that the EPR spectrum at 77 or 10 K shows a predominant low-spin heme population for CCP, we have examined the temperature variation of the single-crystal RR spectra using a Joule-Thompson cryostat attachment to the microscope stage. For these experiments the crystals were examined in sealed capillaries to prevent lyophilization in the cryostat vacuum chamber. At low temperatures the spectrum converts partially to one which is characteristic of low-spin Fe^{III} heme. The conversion is very gradual, however, and is incomplete even at −190 °C. We infer that lowering the temperature produces a gradual change in the protein structure which increasingly permits the Fe^{III} atom to approach the heme plane and bind a distal ligand, either the distal water molecule or the distal histidine residue. The transition is completely reversible, the native spectrum being regained when the sample is warmed back to room temperature.

Experimental Procedures

Materials and Methods. Cytochrome *c* peroxidase (CCP) was purified from bakers's yeast according to published procedures (Nelson et al., 1977). Single crystals were grown by vapor equilibrium of 15-μL sitting drops of 10 mg/mL protein in 0.05 M potassium phosphate, pH 6.0, 20% 2-methyl-2,4-pentanediol against a reservoir of 0.05M potassium phosphate and 30% methylpentanediol. Crystallization was induced by transferring a single, partially dissolved microcrystal into each protein-solution drop (Thaller et al., 1981). This seeding technique produces crystals that are consistently more resistant to cracking as a result of temperature change than crystals grown by conventional batch methods.

Aqueous Solution. A solution sample of CCP was obtained by dissolving a single crystal with 1–5 μL of phosphate buffer solution. The concentration is estimated to be in the range 1–3 mM. The Raman spectra were measured on the microscope stage with the solution in a capillary or under the cover glass as a hanging drop. With the low laser power and high collecting efficiency of our microprobe system, good spectra can be obtained in 5 min for such a stationary sample and no photodamage can be seen after 20–30 min in the beam.

Single Crystal. The CCP crystal was mounted with a small amount of mother liquor in a sandwich of two cover glasses sealed by vacuum grease. The assembly was attached to the rotating stage of the microscope, which was mounted as part of the optical system of the Raman spectrometer, as shown in Figure 1. The laser power on the crystal surface was estimated to be ~500 mW/mm² with 441.6-nm excitation. The incident laser power was ~10 mW and was attenuated by a 1.5 OD neutral density filter. In addition, a polarizer also attenuated the power, by a factor of 4. Consequently, 5% of the incident power was reflected down to the crystal. If higher power was used or if the crystal was removed from the mother liquor, there were clear indications of photoreduced species in the Raman spectra. At room temperature, average

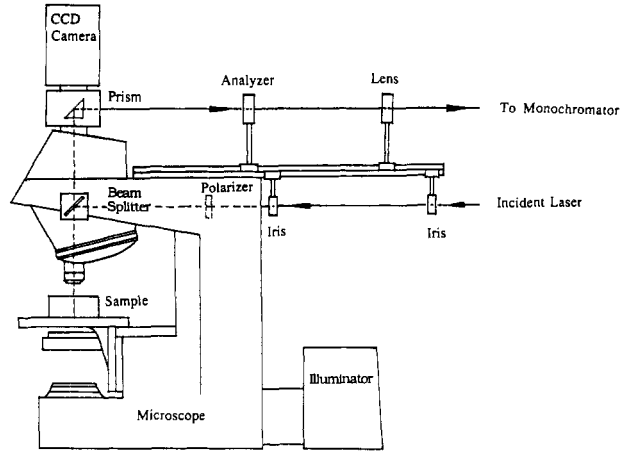

FIGURE 1: Schematic representation of the Raman microprobe apparatus.

spectra were obtained from sevral different nearby spots. For polarization studies the accumulation time at each spot was divided between alternating parallel and perpendicular collection. The order was reversed for successive spots to minimize photoinduced artifacts. Ten spectra with 1-min accumulation time each were added. The Raman frequencies were calibrated relative to those of indene taken under the same conditions.

A Joule-Thompson cryostat from MMR Technology, Inc., was used for low-temperature spectroscopy. The temperature of the cooling stage can be controlled from +50 to −191 °C with an accuracy of ±2 °C. The system requires a vacuum for low-temperature operation. To prevent dehydration of the protein crystal in the vacuum chamber, we enclosed the protein crystal along with some mother liquor in a small capillary, about 15 mm long. The sealed capillary was then mounted on the gold-coated cooling plate with thermally conductive grease. At each temperature the sample was equilibrated for at least 15 min. Both the vacuum hose and cryostat can be fixed to the optical table and microscope stage to minimize vibrations.

Raman Microprobe. The Raman microprobe apparatus is schematically presented in Figure 1. The system includes a laser light source (Spectra-Physics Model 2025 Ar^+ or Liconix He–Cd) and a Spex Model 1401 double monochromator with the center slit replaced by a larger diaphragm to increase the spectral coverage. The fore optics includes a Zeiss Axioskope infinity-corrected microscope with a beam splitter and filter carrier. The beam splitter used in this study reflects only 5% of the incoming laser light. The laser was focused onto the sample with an Olympus infinity-corrected ULWD (Ultra Long Working Distance) objective which is capable of ×80 magnification with 0.75 numeric aperture and 4.1-mm working distance, compatible with the cooling device. The Raman signal is also collected through the same objective in a 180° collecting geometry. With tight focusing, the laser spot was estimated (via the combined magnification of the objective lens and eye piece) to be ≤1 μm. However, Raman spectra were obtained with a slightly defocused laser (~3 μm) to prevent photoinduced damage. An intensified silicon photodiode-array multichannel detector from Princeton Instruments was used for data collection, and the frequency scale was calibrated with an indene sample in the microprobe.

Results and Discussion

RR Spectra. Figures 2 and 3 show CCP RR spectra in the 1300–1700-cm^{-1} region with 441.6- and 514.5-nm laser excitation. The latter is in resonance with the heme Q bands,

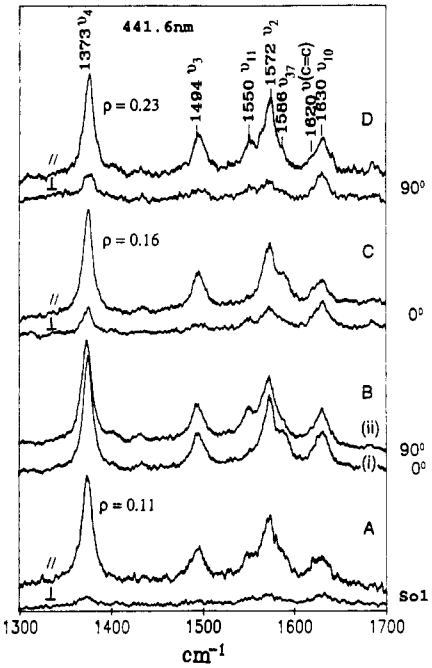

FIGURE 2: Resonance Raman spectra of CCP obtained with 441.6-nm excitation. (A) Solution spectra taken in parallel and perpendicular polarization. (B) (i) Resonance Raman spectrum of a CCP single crystal obtained with the laser polarization parallel (0°) to the *c* axis of the crystal and (ii) with the laser polarization perpendicular (90°) to the *c* axis of the crystal. (C) Polarized spectra obtained at 0° to the *c* axis, with scattering components analyzed parallel and perpendicular to the laser. (D) Polarized spectra obtained at 90° to the *c* axis. The measured depolarization ratio ($\rho = \perp/\parallel$) is given for the 1373 cm^{-1} Raman band.

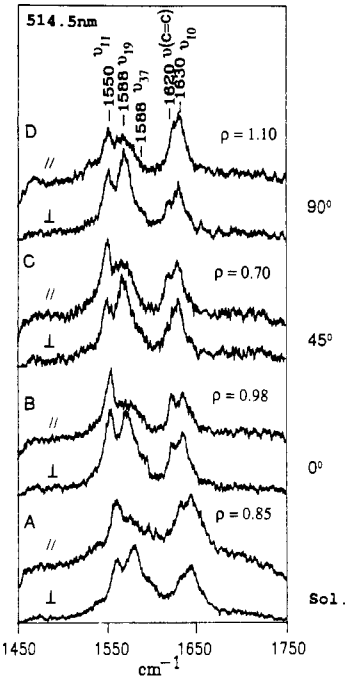

FIGURE 3: Resonance Raman spectra of CCP obtained with 514.5-nm excitation. (A) Solution spectra taken in parallel and perpendicular polarization. (B–D) Polarized spectra of a CCP single crystal in different orientations. The angles of the crystal *c* axis relative to the laser polarization are shown. The measured depolarization ratio ($\rho = \perp/\parallel$) is given for the 1550-cm^{-1} Raman band.

while the former is near resonance with the very strong Soret band (λ_{max} = 408 nm). (Attempts to obtain crystal spectra even closer to resonance, with 413.1-nm Kr^+ laser excitation, were unsuccessful due to excessive light absorption.) Q band resonance enhances non totally symmetric modes via the B-term (vibronic mixing) mechanism (Spiro & Li, 1988). Especially prominent with 514.5-nm excitation are the B_{1g} porphyrin skeletal modes, ν_{10} and ν_{11}, at 1630 and 1550 cm^{-1}, and the A_{2g} modes at 1568 cm^{-1}. These symmetry designations are for the D_{4h} point group, which is a good approximate classification for the heme chromophore, as shown by the fact that the depolarization ratio, $\rho = I_\perp/I_\parallel$ (ratio of scattering intensity analyzed perpendicular and parallel to the incident laser vector), is within experimental error of the expected D_{4h} value, 0.75, for the ν_{10} and ν_{11} bands of CCP in solution (bottom panel of Figure 3), while ν_{19} is anomalously polarized ($\rho > {}^3/_4$) also as expected (Li & Spiro, 1988). Symmetry lowering effects are seen, however, in (a) the nonzero value for $I_\parallel$ of ν_{19} and (b) the appearance of a band due to an E_u mode, ν_{37} (1586 cm^{-1}), activated due to the loss of the electronic symmetry center by the asymmetrically disposed vinyl substituents, and a band at 1620 cm^{-1} arising from the C=C double bond stretch of the vinyl groups themselves (Choi et al., 1982). It is interesting that these bands are seen with Q-band excitation, since they had been thought to be selectively enhanced via Soret excitation; they are brought out clearly in the crystal spectra.

Table I: Correlation Diagram for the Scattering Tensor Elements among the Molecular Site and Factor Groups

	D_{4h}	C_1	D_2
$\alpha_{xx} + \alpha_{yy}$	A_{1g}	A	A α_{aa}, α_{bb}, α_{cc}
$\alpha_{xx} - \alpha_{yy}$	B_{1g}		B_1 α_{ab}
$\alpha_{xy} - \alpha_{yx}$	A_{2g}		B_2 α_{ac}
$\alpha_{xy} + \alpha_{yx}$	B_{2g}		B_3 α_{bc}

With excitation near the Soret band (Figure 2) totally symmetric (A_{1g}) modes are enhanced via the dominant A term (Franck–Condon) scattering mechanism (Spiro & Li, 1988), especially ν_4, ν_3, and ν_2, at 1373, 1494, and 1572 cm^{-1}. The ν_4 depolarization ratio in solution (bottom panel) is again within experimental error of the value, 0.125, expected for an A_{1g} mode in resonance with an in-plane electronic transition ($\alpha_{xx} = \alpha_{yy}$, $\alpha_{zz} = 0$). The B_{1g} modes ν_{10} and ν_{11} (but not the A_{2g} mode, ν_{19}) are also activated, via a Jahn–Teller effect in the degenerate Soret excited state (Cheung et al., 1978), and the ν_{37} (E_u) and vinyl ν(C=C) bands are also seen.

Orientation Effects. The upper panels of Figures 2 and 3 show RR spectra obtained with the laser electric vector aligned perpendicular (90°), parallel (0°), and at 45° (514.5-nm excitation, Figure 3) to the long axis, *c*, of the CCP crystal, which lay on its 110 face. Both parallel and perpendicular components ($\parallel$ and $\perp$) of the scattered light are shown. With 441.6-nm excitation substantial differences in relative intensity are seen in the parallel spectra, which are compared directly in panel B of Figure 2. Relative to the A_{1g} bands, the B_{1g} bands are selectively enhanced in the 0° spectrum, while the E_u and ν(C=C) bands are selectively enhanced at 90°. Moreover, the depolarization ratio of the individual bands varies with the crystal orientation for both sets of spectra.

These orientational effects are associated with the symmetry properties of the normal mode scattering tensors with respect to the molecular and crystal framework. Since the heme chromophores are vibrationally well isolated one from another, the crystal scattering tensors are obtained from the molecular scattering tensors via the direction cosine transformation matrix and summing over the molecules in the unit cell (Sage et al., 1989). CCP crystallizes in the space group $P2_12_12_1$ (factor group D_2) with four molecules in general positions (Poulos et al., 1980). The correlation of the scattering elements, α, between molecular axes (*x*, *y*, *z*) and crystal axes (*a*, *b*, *c*) is given in Table I for the in-plane Raman modes of

Table II: Geometric Relations between Crystal and D_{4h} Heme In-Plane Tensor Elements[a]

Mode Symmetry	
A_{1g}	$\alpha_{ij} = f_{ij}(\alpha_{xx} + \alpha_{yy})$; $f_{ii} = i_x^2 + i_y^2$; $f_{i\neq j} = i_xj_x + i_yj_y$
B_{1g}	$\alpha_{ij} = f_{ij}(\alpha_{xx} - \alpha_{yy})$; $f_{ii} = i_x^2 - i_y^2$; $f_{i\neq j} = i_xj_x - i_yi_y$
B_{2g}	$\alpha_{ij} = f_{ij}(\alpha_{xy})$; $f_{ii} = 2i_xi_y$; $f_{i\neq j} = i_xj_y + i_yj_x$
A_{2g}	$\alpha_{ij} = f_{ij}(\alpha_{xy})$; $f_{ii} = i_xi_y - i_yi_x = 0$; $f_{i\neq j} = i_xj_y - i_yj_x$

Direction Cosines as Functions of the Eulerian Angles[b]

$a_x = \cos\gamma\cos\varphi\cos\chi - \sin\varphi\sin\chi$
$a_y = -\cos\gamma\cos\varphi\sin\chi - \sin\varphi\cos\chi$
$b_x = \cos\gamma\sin\varphi\cos\chi + \cos\varphi\sin\chi$
$b_y = -\cos\gamma\sin\varphi\sin\chi + \cos\varphi\cos\chi$
$c_x = -\sin\gamma\cos\chi$
$c_y = \sin\gamma\sin\chi$

[a] See Suzuki et al. (1968). [b] γ is the angle from the *c* crystal axis to the heme normal, *z*. φ is the angle from the *a* axis to the projection of *z* onto the *ab* plane. χ is the angle in the heme plane, *xy*, between the *y* axis and the intersection of the heme plane with the *ab* crystal plane.

a D_{4h} chromophore. Geometric relationships connecting molecular and crystal (α_{ij}) tensor elements are given in Table II. These are expressed in terms of the direction cosines between the molecular and crystal axes, $i_{x,y}$, $j_{x,y}$, where i,j = *a*,*b*, or *c*. As also described in Table II, the direction cosines can in turn be expressed in terms of the three Eulerian angles (Wilson et al., 1980), γ, φ, and χ, which describe the heme plane. Since the molecular polarizability tensors are constants of the molecule, the intensity variations with crystal orientation are contained in the direction cosine functions, f_{ij}. In addition, the intensities are subject to self-absorption corrections, which also vary with the orientation, and are hard to estimate. These corrections nearly cancel (Sage et al., 1989) in the depolarization ratios, however, which can be calculated from the appropriate expressions in Table II. For example, if the crystal were lying on its *ab* (001) face, the depolarization ratio with the laser vector in the *a* direction would be $\rho_a = \alpha_{ab}^2/\alpha_{aa}^2$, while in the *b* direction it would be $\rho_b = \alpha_{ab}^2/\alpha_{bb}^2$. In the present case the crystal shows its 110 face with *b* and *a* axes tilted by an angle ϑ (=54.45°) with respect to the plane of the microscope stage and to its normal, respectively. Consequently, the expressions for ρ along the crystal axes must be transformed via a rotation matrix, to give

$$\rho_a = \alpha_{a'c}^2/\alpha_{a'a'}^2;\ \rho_c = \alpha_{a'c}^2/\alpha_{cc}^2$$

where

$$\alpha_{a'a'} = \alpha_{aa}\cos^2\vartheta + \alpha_{bb}\sin^2\vartheta + 2\alpha_{ab}\sin\vartheta\cos\vartheta$$

$$\alpha_{a'c} = \alpha_{ac}\cos\vartheta - \alpha_{bc}\sin\vartheta$$

$$\alpha_{c'c'} = \alpha_{cc}$$

The required orientation angles of the heme groups are available from the crystal structure (Poulos et al., 1980) and are listed in Table III, along with experimental and calculated ρ values for 0° and 90° crystal orientations of three bands: the 1373-cm^{-1} ν_4 band excited at 441.6 nm and the 1630- and 1550-cm^{-1} ν_{10} and ν_{11} bands as well as the 1620-cm^{-1} $\nu_{C=C}$ vinyl band excited at 514.5 nm. The calculated ρ values are in excellent agreement with experiment for ν_4 (A_{1g}) but show very large discrepancies for the remaining bands when they are treated as arising from B_{1g} modes. We were able, however, to bring the calculated values into satisfactory agreement by allowing χ to vary for each mode. Table III also lists these adjusted values and the optimum χ angles to which they correspond. For ν_{11}, ν_{10}, and $\nu_{C=C}$, χ_{opt} = 122°, 140°, and 119°, whereas the crystallographic χ is 74°, taken as the average of the two values, 77.8° and 65.9°, given by the coordinates of the four N atoms of the pyrrole rings.

We interpret these results as follows. Because the A_{1g} modes are totally symmetric, their intensities are sensitive only to the

Table III: Calculated[a] and Experimental[b] Depolarization Ratios for CCP Single-Crystal Orientation[c]

crystal orientation	0°	90°
A_{1g}, calc (χ = 74°)	0.15	0.23
ν_4, exp	0.16	0.23
B_{1g}, calc (χ = 74°)	0.05	0.09
ν_{11}, exp	0.98	1.10
calc (χ = 122°)	0.95	1.10
ν_{10}, exp	0.57	1.28
calc (χ = 140°)	0.42	1.24
$\nu_{C=C}$, exp	0.76	0.76
calc (χ = 119°)	0.71	0.84

[a] Calculations based on D_{4h} symmetry and the geometric relations described in the text, with γ = 116.1°, φ = 40°, and χ = 74° (average of 66° and 78° values from the four pyrrole N atomic coordinates; Poulos et al., 1980), or for the indicated χ values optimized to give the best agreement with experiment. [b] ν_4 measured with 441.6-nm excitation; ν_{11}, ν_{10}, and $\nu_{C=C}$ measured with 514.5-nm excitation. [c] Angle of the *c* crystal axis relative to the laser electric vector when the beam was directed along the normal to the 110 face.

γ and φ angles, which define the heme normal, and not to the χ angle, which defines the *x* and *y* axes in the plane. The good agreement with the A_{1g} ρ values means that the crystal is well oriented, that *x* and *y* directions in the ring are equivalent ($\alpha_{xx} = \alpha_{yy}$), and that the out-of-plane tensor component, α_{zz}, is negligible, as is also indicated by the solution depolarization ratio. The non totally symmetric mode intensities are highly dependent on χ, however.

The B_{1g} classification (tensor $\alpha_{xx} = \alpha_{yy}$) of ν_{10} and ν_{11} defines the *x* axis as lying along a line connecting opposite pyrrole atoms. These modes are known from vibrational analysis (Spiro & Li, 1988) to be symmetric with respect to this axis, whereas the B_{2g} modes (α_{xy}) are antisymmetric. (If the *x* axis were instead identified with the line connecting the opposite methine bridges, ν_{10} and ν_{11} would become B_{2g} modes.) The fact that χ_{opt} deviates markedly from the N–N directions implies a reduction in symmetry and a rotation of the in-plane electronic transition moments away from these directions. The effect of this rotation is to induce nonzero α_{xy} scattering elements into the nominally B_{1g} scattering tensor, giving the modes some B_{2g} character. For the ν_{11} mode this substitution is complete, since χ_{opt} is 45° (within experimental error) from the N–N direction; i.e., the transition moment actually lies along the C_m–C_m direction (C_m is the methine carbon atom). The dominant tensor element is now α_{xy}. (The same ρ values are calculated by using the B_{2g} mode geometric relations and the N–N direction for χ.)

The symmetry lowering may be due to the asymmetric disposition of the porphyrin substituents or to electrostatic asymmetry in the protein surroundings. Because the transition dipole appears to line up along a C_m–C_m direction, it is tempting to invoke the vinyl groups as the perturbing influence, since they are aligned roughly along one of these directions. (We cannot distinguish between the two C_m–C_m directions, however, since ρ is periodic in χ, with a period of 90°.)

Other symmetry-lowering effects might be anticipated, including nonequivalence and nonorthogonality of the *x*,*y* transition moments and differential tensor element enhancement due to *x*,*y* energy splitting in the excited state, as well as nonzero values for out-of-plane elements, α_{zz}, α_{xz}, α_{yz}. Some of these effects have been examined systematically by Sage et al. (1989) in the context of A_{1g} depolarization ratios of myoglobin crystals. The fact that the ν_4 (A_{1g}) depolarization ratios are correctly predicted on the basis of the crystal structure data indicates, however, that *x*,*y* inequivalence cannot be large and that out-of-plane elements are small.

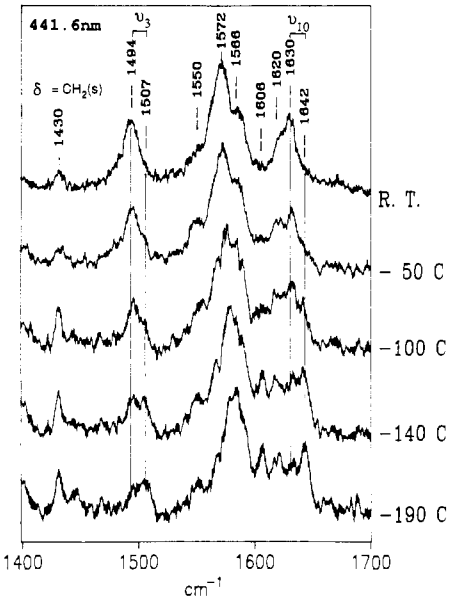

FIGURE 4: Resonance Raman spectra of a CCP single crystal obtained with 441.6-nm excitation (at 0° to the *c* axis without an analyzer) at different temperatures.

The situation is more complex for the ν_{10} and vinyl modes. These bands overlap substantially, and indeed it seems likely that the vinyl mode gains its intensity by borrowing from ν_{10} via a near resonant interaction (Fermi resonance). In low-spin forms of CCP and its mutants ν_{10} is shifted to higher frequency (1638 cm^{-1}), and the vinyl band is not seen with Q band excitation (Smulevich et al., 1988, 1989). It is for this reason that we treated the vinyl mode in terms of B_{1g} symmetry. Because of the overlap, the experimental ρ values are less certain than for ν_{11}; the envelope was deconvoluted by using Lorentzian band shapes, and ρ was calculated from the peak heights of the resolved components. Nevertheless, ρ is clearly different for ν_{11} and for the vinyl and ν_{10} bands, as can be seen by visual inspection of Figure 3, and the χ_{opt} for ν_{11} does not give a satisfactory account of the data. The χ_{opt} values that give the best agreement deviate from the ν_{11} χ_{opt} by $-3°$ for the vinyl mode and $+18°$ for ν_{10}. It is possible that these deviations arise from the same near-resonant interaction that leads to intensity sharing between ν_{10} and the vinyl mode. If the electronic transition moment is along the C_m–C_m direction, as suggested by the ν_{11} data, giving a basically B_{2g} character to the nominally B_{1g} modes, then we speculate that the vinyl ν_{10} mode interaction might have the effect of reintroducing B_{1g} character ($\alpha_{xx} = \alpha_{yy}$ elements) of opposite phase and variable magnitude, producing the apparent rotations in χ_{opt}.

In summary, the crystal depolarization ratios indicate that the *x* and *y* transition moments of the heme group are equivalent and orthogonal in CCP, but their orientation is along the C_m–C_m rather than the N–N directions, perhaps because of electronic steering by the vinyl groups. The apparent orientation is different for the ν_{10} and vinyl modes, perhaps because of their near-resonant interaction.

Low-Temperature Spectra. Figure 4 shows spectra of a CCP single crystal (0° orientation) obtained at various temperatures with the Joule-Thompson cryostat on the microscope stage. As the temperature is lowered, the spectrum is converted partially to one in which the mode frequencies are significantly higher than those in the room temperature spectrum. This is seen most clearly for ν_3 and ν_{10}, marked by the vertical lines on the figure. The overlapping bands in the 1550–1620-cm^{-1} region make assignments difficult, but similar trends are apparent. The high ν_3 (1507 cm^{-1}) and ν_{10} (1642 cm^{-1}) frequencies of the new spectrum are characteristic either of low-spin or of intermediate-spin Fe^{III} hemes (spiro & Li, 1988). Both forms have similarly contracted porphyrin cores, because of the empty in-plane antibonding iron orbital $d_{x^2-y^2}$, and therefore have similar frequencies for the core size marker bands which are monitored in the present experiment. A low-spin heme requires coordination by two axial ligands, with a ligand field strong enough to force pairing of the iron electrons in the d_π orbitals. An intermediate-spin heme, on the other hand, requires a very weak axial field, allowing the iron electrons to distribute themselves in four nonbonding d orbitals (including d_{z^2}), leaving only the in-plane $d_{x^2-y^2}$ orbital empty. Similarly, high ν_3 and ν_{10} frequencies were observed for the analogous protein horseradish peroxidase (HRP) at low temperature (Evangelista-Kirkup et al., 1985) and were attributed to an intermediate-spin state in accordance with previous EPR evidence (Maltempo et al., 1979). A weakened iron–proximal imidazole linkage at low temperature was inferred.

For CCP, however, Yonetani and Anni (1987) have provided clear EPR evidence for a low-spin state at low temperature. We therefore assign the partially formed low-temperature spectrum to a low-spin species. In a previous paper from this laboratory (Evangelista-Kirkup et al., 1985), a six-coordinate high-spin heme RR spectrum was found for solutions of CCP frozen to 77 or 9 K. Yonetani and Anni (1987), however, have shown that a high-spin EPR signal at low temperature is associated with aging of the CCP. Consistent with this observation, we have since found that low-temperature RR spectra of fresh CCP solutions likewise give mainly low-spin rather than six-coordinate high-spin signals (Smulevich et al., 1989).

The CCP X-ray crystal structure shows the Fe atom located 0.2 Å out of the heme plane on the proximal side (Poulos et al., 1980; Finzel et al., 1984). The distal water molecule sits directly above the Fe atom, but at a distance, 2.4 Å, that precludes a strong interaction. The RR spectra, establishing a five-coordinate high-spin heme in solution as well as in the crystal, provide direct evidence that there is no significant interaction between the Fe atom and the distal water molecule at room temperature. Conversion of the RR spectrum to one characteristic of a low-spin heme at low temperature implies that the Fe atom approaches the heme plane and that a sixth ligand is bound. The plausible candidates for this sixth ligand are the distal water molecule or the distal histidine residue, His-52. While the histidine coordination would definitely produce a low-spin heme, the His-52 side chain is rather far from the Fe atom at room temperature (3.3 Å) (Finzel et al., 1984), and appreciable reorganization of the protein would be required to permit its binding. The spin state in the case of a water molecule sixth ligand is harder to predict. For metaquomyoglobin or hemoglobin a mixture of high- and low-spin six-coordinate heme is observed (Iizuka & Kotani, 1968, 1969a,b). The high-spin form predominates at room temperature, but lowering the temperature favors the low-spin form. At no temperature do we see any evidence for six-coordinate high-spin signals (ν_3 = 1477 cm^{-1}, ν_{10} = 1615 cm^{-1}) (Smulevich et al., 1986a). Since, however, the low-spin RR signature begins to appear only at −50 °C and below, it is possible that water is the sixth ligand and that the high-spin six-coordinate form is missed because binding only occurs at temperatures where this form is unstable relative to the low-spin form.

It is also conceivable that the sixth ligand is hydroxide formed by ionization of the bound water molecule due to an

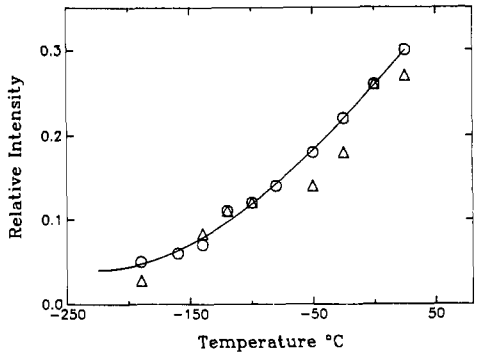

FIGURE 5: Raman intensity ratios of the 1494/1373 (O) and 1630/1373 cm^{-1} (Δ) bands vs temperature. The curve presents the best fit to the data.

increase in pH at low temperatures. It is known (Douzou, 1977) that a pH 7.36 phosphate buffer in 50% MPD shows a 0.5-unit increase in pH when it is cooled from 20 to −25 °C. The CCP crystals were bathed in a phosphate buffer in 30% MPD, pH 6.3. In aqueous buffer the transition to the alkaline form of CCP occurs at pH 7.5 (Shelnutt et al., 1983). Whether the effective pH could reach this range at the lowest temperatures is uncertain. However, this seems unlikely since crystals of a mutant CCP, Phe-51, have been observed to remain high spin at low temperature despite having an acid–alkaline transition in the same range as CCP (Smulevich et al., 1989).

An interesting additional feature of the low-temperature spectra is the sharpening of the band at 1430 cm^{-1}, which is assigned (Choi et al., 1982) to a scissors mode of the vinyl CH_2 group. We infer that there is a tightening of the environment around one or both vinyl groups that diminish the inhomogeneous broadening evident at room temperature. Possibly, the orientation relative to the heme plane also changes for one or both vinyl groups, making them more equivalent at low temperature.

The conversion of the five-coordinate spectrum to the low-spin six-coordinate spectrum is very gradual. It sets in at −50 °C but a fraction of high-spin signal remains even at −190 °C. In Figure 5, the decreasing intensities of the five-coordinate bands ν_3 and ν_{10}, relative to the intensity of the ν_4 (1373 cm^{-1}) band (whose frequency is independent of the spin state), are plotted against temperature. The process is completely reversible, and the original spectrum is reestablished when the sample is warmed to room temperature. Thus, there is no phase change in the protein crystal and no temperature at which the structure suddenly changes. Rather, the effect seems to be a steady increase in the protein packing forces with decreasing temperature, or equivalently a decrease in fluctuations which overcome these forces, allowing the Fe atom to approach the heme plane and bind the distal ligand. These forces are not without biological interest since the same motion of the Fe atom into the heme plane must occur during enzyme turnover as the substrate, hydrogen peroxide, is bound and activated and the product, water, is released.

Conclusions

A Raman microscope is shown to be an effective instrument for obtaining protein single-crystal Raman spectra under resonance conditions. Distinctive orientation and polarization effects are seen which are useful in discriminating Raman bands, on the basis of their symmetry. Isolated A_{1g} (ν_4) and B_{1g} (ν_{11}) modes give depolarization ratios that are accurately calculated with a D_{4h} model, provided that the electronic transition moments are assumed to lie along the C_m–C_m directions. Deviations are seen for the ν_{10} and vinyl modes, however, which may arise from their interaction. RR spectroscopy shows CCP to be five coordinate, both in solution and in single crystals, confirming that the distal water molecule seen in the X-ray structure is not bound to the Fe at room temperature. As the temperature is lowered, partial conversion to a low-spin heme is seen, suggesting that the distal water or the distal histidine is partially bound at low temperature and that thermal effects maintain the five-coordinate state at room temperature.

Acknowledgments

We are grateful to Professor Mario Marzocchi for his interest and guidance with respect to the tensor calculations.

References

Carey, P. R. (1982) *Biochemical Applications of Raman and Resonance Raman Spectroscopies*, Academic Press, New York.

Cheung, L. D., Yu, N.-T., & Felton, R. H. (1978) *Chem. Phys. Lett. 55*, 527.

Choi, S., Spiro, T. G., Langry, K. C., Smith, K. M., Budd, D. L., & LaMar, G. N. (1982) *J. Am. Chem. Soc. 104*, 4345.

Dasgupta, S., Rousseau, D. L., Anni, H., & Yonetani, T. (1989) *J. Biol. Chem. 264*, 654.

Douzou, P. (1977) *Cryobiochemistry*, p 56, Academic Press, London.

Evangelista-Kirkup, R., Crisanti, M., Poulos, T. L., & Spiro, T. G. (1985) *FEBS Lett. 190*, 221.

Finzel, B. C., Poulos, T. L., & Kraut, J. (1984) *J. Biol. Chem. 259*, 113027.

Hashimoto, S., Tatsuno, Y., & Kitagawa, T. (1986a) *Proc. Natl. Acad. Sci. U.S.A. 83*, 2417.

Hashimoto, S., Teraoka, J., Inubushi, T., Yonetani, T., & Kitagawa, T. (1986b) *J. Biol. Chem. 261*, 11110.

Iizuka, T., & Kotani, M. (1968) *Biochim. Biophys. Acta 167*, 257.

Iizuka, T., & Kotani, M. (1969a) *Biochim. Biophys. Acta 181*, 275.

Iizuka, T., & Kotani, M. (1969b) *Biochim. Biophys. Acta 194*, 351.

Loppnow, G. R., & Mathies, R. A. (1989) *Rev. Sci. Instrum. 60*, 2628–2630.

Loppnow, G. R., Barry, B. A., & Mathies, R. A. (1989) *Proc. Natl. Acad. Sci. U.S.A. 86*, 1515–1518.

Maltempo, M. M., Ohisson, P.-I., Paul, K.-G., Petersson, L., & Ehrenberg, A. (1979) *Biochemistry 18*, 2935.

Morikis, D., Sage, J. T., Rizos, A. K., & Champion, P. M. (1988) *J. Am. Chem. Soc. 110*, 6341.

Nelson, C. E., Sitzman, E. V., Kang, C. H., & Margoliash, E. (1977) *Anal. Biochem. 83*, 622–631.

Poulos, T. L., Freer, S. T., Alden, R. A., Edwards, S. L., Skogland, U., Takio, K., Eriksson, B., Xuong, N., Yonetani, T., & Kraut, J. (1980) *J. Biol. Chem. 255*, 575.

Sage, J. T., Morikis, D., & Champion, P. M. (1989) *J. Chem. Phys. 90*, 3015–3032.

Shelnutt, J. A., Satterlee, J. D., & Erman, J. E. (1983) *J. Biol. Chem. 258*, 2168.

Smulevich, G., Evangelista-Kirkup, R., English, A., & Spiro, T. G. (1986a) *Biochemistry 25*, 4426.

Smulevich, G., Dasgupta, S., English, A., & Spiro, T. G., (1986b) *Biochim. Biophys. Acta 873*, 88.

Smulevich, G., Mauro, J. M., Fishel, L. A., English, A. M., Kraut, J., & Spiro, T. G. (1988) *Biochemistry 27*, 5477.

Smulevich, G., Mantini, A. R., English, A. M., & Mauro, J.

M. (1989) *Biochemistry 28*, 5058.
Spiro, T. G., & Li, X.-Y. (1988) in *Biological Applications of Raman Spectroscopy*, Vol. 3, Chapter 1, Wiley-Interscience, New York.
Suzuki, M., Yokoyama, T., & Ito, M. (1968) *Spectrochim. Acta 24A*, 1091.
Thaller, C., Weaver, L. H., Eichele, G., Wilson, E., Karlsson, R., & Jansonius, J. N. (1981) *J. Mol. Biol. 147*, 465-469.
Wilson, E. B., Jr., Decius, J. C., & Cross, P. C. (1980) *Molecular Vibrations*, Dover Publications, New York.
Yonetani, T. (1976) *Enzymes (3rd Ed.) 13*, 345-361.
Yonetani, T., & Anni, H. (1987) *J. Biol. Chem. 262*, 9547.

Structure of a Thermostable Disulfide-Bridge Mutant of Phage T4 Lysozyme Shows That an Engineered Cross-Link in a Flexible Region Does Not Increase the Rigidity of the Folded Protein[†,‡]

P. E. Pjura, M. Matsumura, J. A. Wozniak, and B. W. Matthews*
Institute of Molecular Biology and Department of Physics, University of Oregon, Eugene, Oregon 97403
Received August 16, 1989; Revised Manuscript Received October 12, 1989

ABSTRACT: A disulfide bond introduced between amino acid positions 9 and 164 in phage T4 lysozyme has been shown to significantly increase the stability of the enzyme toward thermal denaturation [Matsumura, M., Becktel, W. J., Levitt, M., & Matthews, B. W. (1989) *Proc. Natl. Acad. Sci. U.S.A. 86*, 6562-6566]. To elucidate the structural features of the engineered disulfide, the crystal structure of the disulfide mutant has been determined at 1.8-Å resolution. Residue 9 lies in the N-terminal α-helix, while residue 164 is located at the extreme C terminus of T4 lysozyme, which is the most mobile part of the molecule. The refined structure shows that the formation of the disulfide bond is accompanied by relatively large ($\sim$2.5 Å) localized shifts in C-terminal main-chain atoms. Comparison of the geometry of the engineered disulfide with those of naturally observed disulfides in proteins shows that the engineered bridge adopts a left-handed spiral conformation with a typical set of dihedral angles and C_α–C_α distance. The geometry of the engineered disulfide suggests that it is slightly more strained than the disulfide of oxidized dithiothreitol but that the strain is within the range observed in naturally occurring disulfides. The wild-type and cross-linked lysozymes have very similar overall crystallographic temperature factors, indicating that the introduction of the disulfide bond does not impose rigidity on the folded protein structure. In particular, residues 162-164 retain high mobility in the mutant structure, consistent with the idea that stabilization of the protein is due to the effect of the disulfide cross-link on the unfolded rather than the folded state. The 9-164 disulfide bridge, as well as other disulfides in T4 lysozyme, were introduced into a pseudo-wild-type molecule in which the naturally occurring cysteines at positions 54 and 97 were replaced, respectively, with threonine and alanine. The structure of this pseudo-wild-type lysozyme has also been determined at high resolution and shown to be very similar to that of the normal wild-type molecule.

It has been shown for many naturally occurring proteins that disulfide bonds can considerably enhance stability (Anfinsen & Scheraga, 1975; Johnson et al., 1978; Goto & Hamaguchi, 1979; Lin et al., 1984; Ueda et al., 1985; Creighton, 1986; Schwarz et al., 1987; Pace et al., 1988; Lin & Kim, 1989). This large stabilizing potential has made the engineering of nonnative disulfide bonds into proteins an attractive strategy for the improvement of protein stability. Such attempts include dihydrofolate reductase (Villafranca et al., 1983, 1987), T4 lysozyme (Perry & Wetzel, 1984, 1986; Wetzel et al., 1988; Matsumura & Matthews, 1989; Matsumura et al., 1989a,b), subtilisin (Wells & Powers, 1986; Mitchinson & Wells, 1989; Pantoliano et al., 1987), and λ-repressor (Sauer et al., 1986). In all cases the newly introduced cysteines were found to form disulfide bonds, albeit more or less readily in different instances. However, the addition of new disulfides did not always confer an increase in stability relative to that of wild type. One of the reasons for this modest success appears to be the difficulty in finding sites within a protein where the geometry is optimal for introduction of a disulfide bridge. Also, the advantage of the cross-link cannot be fully realized if it leads to proteolysis (Wells & Power, 1986; Mitchinson & Wells, 1989) or intermolecular thiol/disulfide interchange evoked by a third cysteine residue (Perry & Wetzel, 1986; Villafranca et al., 1987).

Recently, four different nonnative disulfide bonds (residues 9-164, 21-142, 90-122, and 127-154) were introduced into a cysteine-free T4 phage lysozyme (Matsumura et al., 1989). The 9-164 and 21-142 disulfide mutants were more thermostable than wild type, whereas the other two mutants were slightly less stable. Measurement of stability of the engineered disulfide bonds to reduction by dithiothreitol (DTT) indicated that the presumed stabilization of the native structure by the reduction in entropy of the unfolded protein (Schellman, 1955; Flory, 1956; Poland & Scheraga, 1965; Chan & Dill, 1989) appeared to be offset by two factors: (1) the disruption or loss of preexisting interactions in wild-type structure due to introduction of new cysteine(s) and (2) the energetic constraints associated with disulfide formation in the native structure. Although the net stability of the engineered protein is determined by the combination of these three factors, from the point

[†] This work was supported in part by a grant from NIH (GM21967 to B.W.M.) and by the Lucille P. Markey Charitable Trust.
[‡] The atomic coordinates in this paper have been submitted to the Brookhaven Protein Data Bank.

0006-2960/90/0429-2592$02.50/0